

# Impedance Estimation of Photovoltaic Modules for Inverter Start-up Analysis

Pallavi Bharadwaj, Abhijit Kulkarni, Vinod John

Department of Electrical Engineering, Indian Institute of Science-Bangalore  
 bharadwaj@ee.iisc.ernet.in, abhijitk@ee.iisc.ernet.in, vjohn@ee.iisc.ernet.in

**Abstract**—Starting-up of photovoltaic (PV) inverters involves pre-charging of the input dc bus capacitance. Ideally, direct pre-charge of this capacitance from the PV modules is possible as the PV modules are current limited. Practically, the parasitic elements of the system such as the PV module capacitance, effective wire inductance and resistance determine the start-up transient. The start-up transient is also affected by the contactor connecting the PV modules to the inverter input dc bus. In this paper, the start-up current and voltages are measured experimentally for different parallel and series connections of the PV modules. These measurements are used to estimate the stray elements, namely the PV module capacitance, effective inductance and resistance. The estimation is based on a linear small-signal model of the start-up conditions. The effect of different connections of the PV modules and the effect of varying irradiation on the scaling of the values of the stray elements is quantified. The analysis of this paper can be used to estimate the expected peak inrush current in PV inverters. It can also be used to arrive at a detailed modelling of PV modules to evaluate the transient behaviour.

**Index Terms**—Photovoltaic module, dynamic model, capacitance, second-order response, cable inductance, irradiation-dependence.

## I. INTRODUCTION

Photovoltaic cell capacitance measurement has drawn attention of researchers in recent times, owing to the importance of dynamically modelling a PV panel, when it interacts with switching converters. Capacitance affects the maximum power point tracking of PV panels [1]. It also causes the flow of inrush current, when a power converter connected to PV, is turned on. If the inrush current is large it can damage the devices of the converter and components such as safety fuses. Also, the parasitic capacitance decides the amount of leakage current to ground and therefore may impact the safety of operating professionals [2]. PV capacitance can be theoretically estimated using p-n junction parameters such as doping [3]. Parasitic capacitance to ground can be analytically estimated using fringe capacitor model [2]. Many methods of experimental evaluation of PV panel's capacitance are reported in literature, such as impedance spectroscopy [3]–[6], voltage ramp method [7]–[9], and transient response measurement [1]. Impedance spectroscopy involves superposition of an ac small signal over a dc bias voltage, the frequency of the ac signal is varied from a few hertz to hundred kHz and the impedance is measured. For silicon solar cells, a frequency range of 1 Hz to 60 kHz is considered sufficient, and a voltage signal of 10–20 mV is superimposed over a dc bias voltage [5], [6]. Often PV impedance measurement experiments, reported in literature

are performed in dark, with voltage applied externally. This however does not reflect the true picture because junction condition is not the same for an irradiated PV panel as compared to a dark panel with voltage applied. Many papers report measurement of capacitance using a reverse dc bias across the solar cell. This again will not give the capacitance of an operating solar cell, as capacitance depends on voltage and a solar cell normally operates under zero bias. As capacitance varies with illumination, voltage and type of solar cell; for a specific application, under given light and bias conditions, it is best determined experimentally. In [1], an external capacitor is connected across a PV panel. The transient current waveform is used to estimate L and C values. However, the first current peak is truncated and the second and third current peak's magnitude and time are used to calculate the parameters. The resultant values of inductance and capacitance parameters are inconsistent with practical values, as reported in [5] to be 0.05  $\mu\text{F}/\text{cm}^2$  capacitance for polycrystalline panels.

In the present work, the PV module impedance is evaluated from the perspective of evaluating the pre-charge current that can occur in a PV array when an inverter dc bus is connected. For this, the experimentally obtained current response is analysed as a simplified second order model. This model is compared with a small signal model of the actual non-linear PV circuit. The values of parameters estimated are seen to be in agreement with practical values, as reported in literature for polycrystalline PV panels [5]. Also, the variation of PV module capacitance with voltage and irradiation is quantified for the present system. Scaling up of capacitance with different series and parallel connection of PV modules is studied along with the effect of cable impedance. Study of this equivalent impedance is crucial to determine the terminal voltage and inrush current, as faced by a power electronic converter, connected to the PV system.

This paper is divided into five sections. System model consisting of the modules, cable and inverter is discussed in Section II. In Section III, experimental results are discussed. Limitations of extending the PV modules analysis to a generic PV array are discussed in Section V. And Section VI concludes the paper.

## II. SYSTEM MODEL

Consider the circuit shown in Fig. 1. It shows the dynamic equivalent circuit of a PV module array, connected through a cable having a resistance,  $R_c$ , and inductance,  $L_c$ , to a converter having a dc bus capacitance,  $C_{inv}$ .

In the PV array model,  $I_g$  shows the light induced current in the PV module,  $I_o$  represents the diode dark saturation current and  $m$  is the diode ideality factor.  $R_{sh}$  and  $R_s$  are the shunt and series resistance, modelling the loss of power within the solar cells of the array. Capacitance  $C$ , models the combined effect of the cell junction and diffusion capacitance, as well as the parasitic capacitance of positive and negative terminals of the PV module to the ground.

Combined series resistance is represented by  $R = R_s + R_c$ , and series inductance is represented by  $L = L_s + L_c$ . Writing

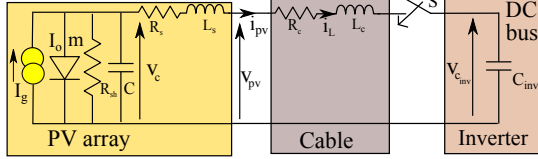


Fig. 1: PV array dynamic model, connected to the dc bus of an inverter, via a connecting cable.

KCL and KVL equations for the circuit shown in Fig. 1 -

$$i_L = I_g - I_o(e^{\frac{v_c}{m n_s V_T}} - 1) - \frac{v_c}{R_{sh}} - C \frac{dv_c}{dt} \quad (1)$$

$$v_c = i_L R + L \frac{di_L}{dt} + v_{c_{inv}} \quad (2)$$

$$i_L = C_{inv} \frac{dv_{c_{inv}}}{dt} \quad (3)$$

#### A. Small signal model

Let  $\bar{x} = [i_L, v_c, v_{c_{inv}}]'$ . Then above equations can be rewritten in  $\dot{\bar{x}} = f(\bar{x})$ , as follows-

$$\frac{di_L}{dt} = -\frac{R}{L} i_L + \frac{v_c}{L} - \frac{v_{c_{inv}}}{L} \quad (4)$$

$$\frac{dv_c}{dt} = -\frac{i_L}{C} - \frac{v_c}{C R_{sh}} - \frac{I_o e^{\frac{v_c}{m n_s V_T}}}{C} + \frac{I_g + I_o}{C} \quad (5)$$

$$\frac{dv_{c_{inv}}}{dt} = \frac{i_L}{C_{inv}} \quad (6)$$

This can further be linearised into the form  $\dot{\bar{x}} = A\bar{x}$  for a linear time invariant system. It can be seen that due to the presence of diode, the equation (5) is non linear. As the dc bus capacitance  $C_{inv}$  is large, its voltage takes time to build up. The circuit emulates a short circuit condition on the PV panel, and this time interval can be considered as a quasi-equilibrium, which is perturbed by LC oscillations. If a small signal analysis is performed to analyse this perturbation, the evaluated partial derivatives, written in the matrix form (7), result in a linear system about every equilibrium point.

$$\Delta \dot{\bar{x}} = \begin{bmatrix} -\frac{R}{L} & \frac{1}{L} & -\frac{1}{L} \\ -\frac{1}{C} & -\frac{1}{C R_{sh}} - \frac{I_o e^{\frac{v_c}{m n_s V_T}}}{C m n_s V_T} & 0 \\ \frac{1}{C_{inv}} & 0 & 0 \end{bmatrix} \times \Delta \bar{x} \quad (7)$$

Another way of arriving at the linear system is by considering only the loops consisting of the linear RLC elements in Fig. 1, that result in oscillatory circuit response, as shown in Fig. 2. Writing KVL and KCL for this circuit, and rearranging into a

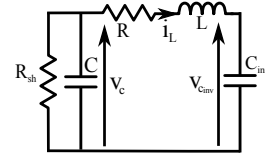


Fig. 2: Simplified circuit showing only linear passive components including three energy storing elements.

state space form one can derive

$$\dot{\bar{x}} = \begin{bmatrix} -\frac{R}{L} & \frac{1}{L} & -\frac{1}{L} \\ -\frac{1}{C} & -\frac{1}{C R_{sh}} & 0 \\ \frac{1}{C_{inv}} & 0 & 0 \end{bmatrix} \times \bar{x} \quad (8)$$

The difference between (8) and (7) is the (2,2) term in RHS matrix. If this term is negligible for the obtained parameter values, the simplified model from Fig. 2 can be used to represent the non-linear model from Fig. 1.

#### B. Simplified second order model

To analyse the response of the circuit shown in Fig. 2, it is analysed in Laplace domain. It must be noted that the presence of  $R_{sh}$  makes the circuit in Fig. 2, a third order system. And, as the value of  $R_{sh}$  is large, it can be ignored and the circuit can be further simplified to a second order system.

Initially the PV terminals are assumed to be open-circuited, and external capacitor is assumed to be uncharged. Therefore, initial conditions for both inductor current and external capacitor voltage remain zero i.e.,  $i_L(0) = 0$  A,  $v_{c_{inv}} = 0$  V. However the PV panel capacitor is charged to the open circuit voltage initially,  $v_c = V_{oc}$ . Inductor current can be written as (9).

$$I_L(s) = \frac{V_{oc}/L}{s^2 + s(R/L) + \frac{1}{LC_s}} \quad (9)$$

where,  $C_s$  is the series equivalent capacitance given by -

$$\frac{1}{C_s} = \frac{1}{C} + \frac{1}{C_{inv}} \quad (10)$$

Time domain solution of (9) can be obtained as

$$i_L(t) = \frac{V_c}{\omega_d L} e^{-\zeta \omega_n t} \sin(\omega_d t) \quad (11)$$

where

$$\omega_n = \frac{1}{\sqrt{LC_s}} \quad (12)$$

$$\zeta = \frac{R}{2\omega_n L} \quad (13)$$

$$\omega_d = \omega_n \sqrt{1 - \zeta^2} \quad (14)$$

Let the first current peak occur at time  $t_1$  and the second peak occur at time  $t_2$ . Since the angle difference between the two consecutive sinusoidal peaks is taken as  $2\pi$ ,  $\omega_n$  in terms of  $\tau_s = t_2 - t_1$  can be written as (15). From measurements  $\tau_s$  is known and  $\omega_n$  can be evaluated. This provides a relationship (12) constraint between  $L$  and  $C_s$ .

$$\omega_n = \frac{2\pi}{\tau_s \sqrt{1 - \zeta^2}} \quad (15)$$

### C. Inductance calculation

At time  $t = 0$ , the current flowing through inductor  $L$  is zero and voltage across capacitor  $C$  is equal to the open circuit voltage. As the initial voltage across external capacitor  $C_{inv}$  and resistor  $R$  is equal to zero, total voltage  $v_c$  comes across the inductor, this can be used to determine  $L$  as shown in (16).

$$L \left. \frac{di_L}{dt} \right|_{t=0} = v_c \Big|_{t=0} \quad (16)$$

Thus if the initial slope is known along with initial PV capacitor voltage, then  $L$  can be computed.

### D. Resistance calculation

Once the oscillations in the transient response has died down and the current has become constant, the voltage drop across the inductor becomes zero, while the voltage across the external capacitor is still negligible, thus all the voltage is dropped across the resistor, which can be evaluated as given in (17).

$$R = \left. \frac{v_C}{i_L} \right|_{\tau_F} \quad (17)$$

where,  $\tau_F$  corresponds to a time when the oscillations have died down. Voltage build-up on  $C_{inv}$  can be written as

$$v_{C_{inv}} \cong \frac{I_{sc} \times t}{C_{inv}} \quad (18)$$

if  $\tau_F \ll \frac{V_{oc} \times C_{inv}}{I_{sc}}$  then it can be approximated that  $v_{C_{inv}} \cong 0$ . If the voltage measurements are made at the cable connection point, marked as  $v_{pv}$  in Fig. 1, then the measured resistance in (17) would correspond to  $R_c$  and not  $R$ .

### E. Capacitance calculation

From (12) - (15), capacitance can be evaluated as

$$C_s = \frac{1}{L \left( \left( \frac{2\pi}{\tau_s} \right)^2 + \left( \frac{R}{2L} \right)^2 \right)} \quad (19)$$

In (19),  $R$ ,  $L$  and  $\tau_s$  are substituted to obtain the equivalent capacitance value of the series RLC circuit. For a linear series R-L-C circuit, the frequency of oscillations should remain fixed as shown by Fig. 3. However, in the case of PV

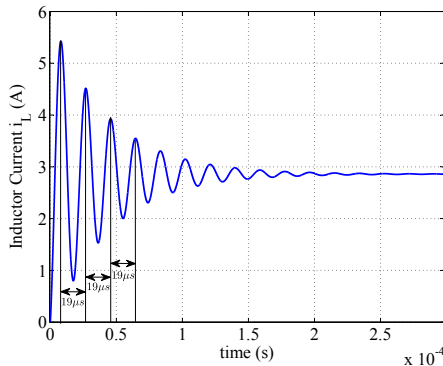


Fig. 3: Simulated current waveform for a linear series R-L-C circuit, showing equal time intervals between subsequent peaks.

inrush current, with the change in terminal voltage, from open

circuit to short circuit, PV capacitance changes resulting in unequal time intervals between first two peaks as compared to subsequent peaks, as discussed in Section V. Since external capacitor  $C_{inv}$  is known, from  $C_s$ , PV capacitance  $C$  can be obtained as

$$C = \frac{C_s C_{inv}}{C_{inv} - C_s} \quad (20)$$

a) *Scaling Up*: If the capacitance obtained above is for a single panel, then it can be scaled up for a PV panel array consisting of several series and parallel connected panels. The method used to find equivalent capacitance is similar to finding the equivalent series and parallel resistances of PV array [10]. If there are  $N_s$  panels in series forming one string and  $N_p$  such strings in parallel,  $C_{eq}$  is given by -

$$C_{eq} = \frac{N_p}{N_s} C \quad (21)$$

Here it is assumed that all the PV panels are identical and therefore have equal capacitance. For an array of PV panels, capacitance  $C$  gets replaced by  $C_{eq}$ , in all the above derived expressions.

## III. EXPERIMENTAL RESULTS AND DISCUSSION

### A. System under study

System under study comprises of 14 polycrystalline PV panels, each rated at 300 W, 40 V. These panels can be connected in different series and parallel combinations. In this paper five configurations are considered namely, I - single panel, II - two panels in series, III - seven parallel panels, IV - seven parallel panels in series with seven parallel panels, and V - fourteen parallel panels. The array capacitance is

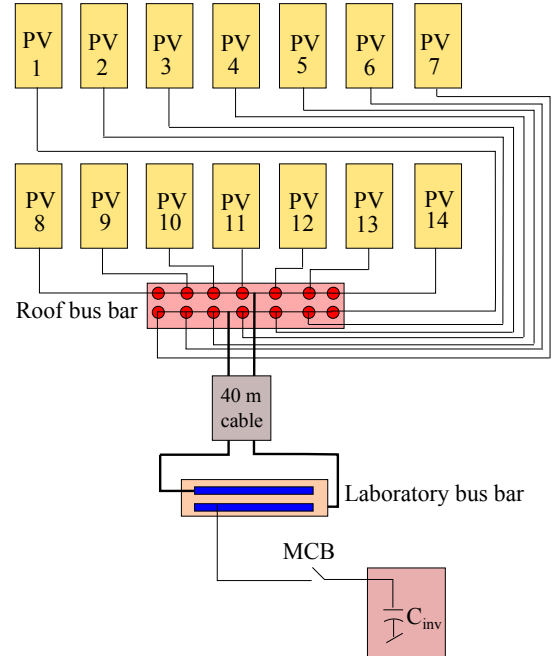


Fig. 4: Single line diagram of PV system, consisting of  $14 \times 300$  W polycrystalline PV panels, connected via cables and bus bar to a 33 mF capacitor through a circuit breaker.

measured by the current response of the circuit when an

external capacitor is connected. The connection is made using a mechanical switch shown as MCB [13] in Fig. 4. It must be noted that the response is different when a solid state switch is used, but in a practical scenario a mechanical switch makes and breaks the contact, and therefore is analysed in the present study.

1) *Single PV panel*: For a single 300 W polycrystalline PV panel, measurements are shown in Fig. 5(a) and Fig. 5(b), which together provide complete response, with Fig. 5(a) captured in  $\mu s$  time scale and Fig. 5(b) captured in  $ms$  time scale. In Fig. 5, the measurements are taken at PV array

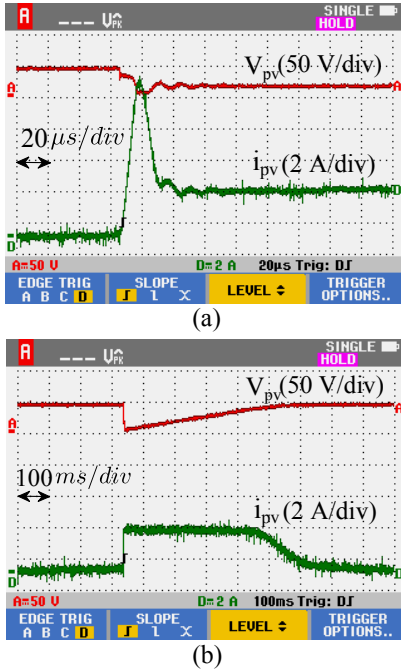


Fig. 5: Measured PV array terminal voltage (A) and current (D) of a PV panel when connected to a capacitor, (a) in  $\mu s$  time scale, (b) in  $ms$  time scale, for a single 300 W PV panel.

terminals as indicated by roof bus bar in Fig. 4. From Fig. 5(a), resistance comes out to be  $4 \Omega$ , from the dc portion of the curve. Inductance value can be evaluated from the initial slope of the current curve, as shown in Fig 5(a). Its value is calculated to be  $86 \mu H$ . By noting the time periods between successive peaks, it can be observed that damped frequency of the system changes. For a linear system, as the damped frequency is a function of R, L and C, it should remain fixed. However, in this case it changes. This is due to the change in PV module capacitance with voltage [5]. Due to charging of external capacitance, PV panel voltage changes from open circuit voltage to zero, at the instant of closing of switch S in Fig. 1, as shown in Fig. 5(b). This causes a corresponding change in panel capacitance. It can further be observed from Fig. 5(a), that the time difference between the first two peaks is significantly higher than the successive peaks, for which it is almost constant. Thus, major change in capacitance occurs only initially, when voltage changes significantly. For this case capacitance comes out to be  $104 \text{ nF}$  from first two peaks and  $60 \text{ nF}$  from second and third peak time difference. It remains almost the same for successive peaks. It should be noted that,

$\frac{R^2}{4L}$  term is much smaller as compared to  $\frac{4\pi^2 L}{T_s^2}$ , and capacitance can be directly approximated as  $C = \frac{T_s^2}{4\pi^2 L}$  in (19). Also, it must be noted that PV panel capacitance is in nF range which is much smaller than  $33 \text{ mF}$  external capacitor  $C_{inv}$ , therefore the series combination of these two is almost equal to PV capacitance, i.e.,  $C_s \cong C$ .

### B. Validation of the simplified second order model

As mentioned in Section II-A, to validate the values of the estimated parameters, R, L and C, the model needs to be validated. The difference between the R-L-C series model and the small signal model of the overall non-linear solar cell model, is the (2,2) term of RHS matrix in (7) and (8). As mentioned in Section II-B,  $R_{sh}$  is also ignored to simplify the system to a second order system, therefore for validation, the effect of  $R_{sh}$  will also be included in the (2,2) term. Evaluating this term using the parameters evaluated for the experimental system, by substituting  $C = 104 \text{ nF}$ ,  $I_o = 0.36 \mu \text{ A}$  [12],  $m = 1.3$  [12],  $R_{sh} = 340 \Omega$ ,  $n_s = 72$  [14] and  $V_T = 26 \text{ mV}$ , the difference term comes out to be

$$-\frac{1}{CR_{sh}} - \frac{I_o e^{\frac{v_c}{m n_s V_T}}}{C m n_s V_T} = -28.3 \times 10^3 - 1.42 e^{\frac{v_c}{2.43}} \quad (22)$$

Assuming voltage drop across PV array series resistance and inductance is negligible, PV capacitance voltage would be approximately equal to the PV array terminal voltage. Substituting  $v_c = 15 \text{ V}$  from Fig. 5(a) and writing complete equation for  $\dot{v}_c$  from (7) and (22)-

$$\dot{v}_c = (-28.3 \times 10^3 - 1.7 \times 10^3) \Delta v_c + 9.6 \times 10^6 \Delta i_L \quad (23)$$

From (23) it can be seen that, the influence of  $\Delta i_L$  term is much more significant, as compared to the  $\Delta v_c$  term, for practical start-up conditions of inverter pre-charge. It can be noted that  $v_c$  falls to zero during the pre-charge duration. It is seen that the difference between the small signal model and the simplified second order model, is insignificant for small values of  $v_c$ . It can be observed from Fig. 5(a) to be true because when the capacitor voltage rises to a significant value, the oscillations subside. Thus the simplified second order model can be used to estimate the parameters of the PV module as suggested in Section II.

1) *Other PV array configurations*: Experimental response for various configuration of PV modules were recorded such as two panels connected in series, seven panels connected in parallel and seven parallel in series with seven parallel panels. Current and voltage response for seven parallel panels case is shown in Fig. 6. Resulting cable resistance and inductance values along with panel capacitance values are tabulated in Table I. It can be observed that, series connection doubles the inductance and resistance, and halves the capacitance value, and vice-versa for parallel connection. However scaling is not exact, this is due to the effect of cable inductance and capacitance, which connects PV panels to the bus bars where the measurements are taken.

### C. Effect of Cable Inductance on scaling

Cable inductance, from roof bus bar to laboratory bus bar, as indicated in Fig. 4, was measured to be  $16 \mu H$  by

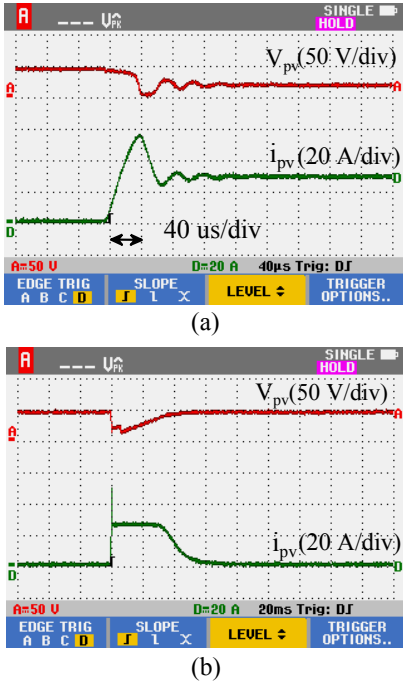


Fig. 6: Measured terminal voltage (A) and current (D) of a PV panel when connected to a capacitor, (a) in  $\mu s$  time scale, (b) in  $ms$  time scale, for seven 300 W PV panels connected in parallel.

LCR meter. Subtracting this value from the overall inductance value, as reported in Table I, roof top panel inductance can be calculated. For single panel case it comes out to be  $70 \mu H$ , from Table I. For the second case, series connection is done in the laboratory, therefore subtracting  $2 \times 16 \mu H$  from 201,  $169 \mu H$  is obtained. This is seen to be more than double the value for single panel owing to the mutual coupling between the cables running from roof to laboratory. For seven parallel case, subtracting  $16 \mu H$ ,  $29 \mu H$  is obtained, which is more than  $70/7 = 10 \mu H$ , this is due to mutual coupling among connecting cables on the roof as shown in Fig. 4. For seven parallel panels in series with seven parallel panels case, inductance is slightly more than double the seven parallel case. This is due to mutual coupling effect, which is missing in the seven parallel case, as only one set of cable is energised.

#### D. Quantifying the error

To quantify the error, per panel capacitance value is derived from array capacitance values as mentioned in Table I. From these per panel values, a constant capacitance value is derived based on least square error from all capacitance values. Taking

TABLE I: Measured resistance, inductance and capacitance values for different PV array configurations

PV Array configuration	R ( $\Omega$ )	L ( $\mu H$ )	$C_{eq}$ (nF)
I	4	86	60
II	7	201	30
III	0.6	45	600
IV	1	94.6	222

the constant value as  $k$  and the individual per panel capacitance values from cases mentioned in Table I as  $C_1, C_2$  etc., error function  $\Pi$  can be formulated as a sum of square of errors.

$$\Pi = (k - C_1)^2 + (k - C_2)^2 + (k - C_3)^2 + (k - C_4)^2 \quad (24)$$

Minimising this error function results into  $k$  being the mean of all capacitance values, given by :

$$k = \frac{C_1 + C_2 + C_3 + C_4}{4} = 68 nF \quad (25)$$

Deviation from this value, gives the error, which is quantified in Table II. It can be noted that configuration III is a clear

TABLE II: Deviation of per panel capacitance from mean value for different PV array configurations

Configuration	Array $C_{eq}$ (nF)	$C_{/panel}$ (nF)	% Error from $k$
I	60	60	-10.8
II	30	60	-10.8
III	600	85.7	27.3
IV	222	63.4	5.8

outlier and therefore is not considered. Average capacitance value  $k$ , now comes out to be  $61.1 nF$ . Recalculated errors are reported in Table III. It shows the error to be within 4%.

TABLE III: Deviation of per panel capacitance from mean value for different PV array configurations, without the outlier

Configuration	Array $C_{eq}$ (nF)	$C_{/panel}$ (nF)	% Error from $k$
I	60	60	-1.8
II	30	60	-1.8
IV	222	63.4	3.8

TABLE IV: Change in array capacitance  $C_{eq}$  with voltage  $V$  for different PV array configurations

PV configuration	$C_{eq_{initial}}$	$C_{eq_{final}}$	$\Delta V_c$	$\frac{\Delta C}{\Delta V}$
I	104 nF	60 nF	39 V	1.1 nF/V
II	67 nF	30 nF	77.3V	1.9 nF/V
III	1200 nF	600 nF	38 V	2.2 nF/V
IV	700 nF	220 nF	75 V	1.8 nF/V

#### E. Variation in capacitance with voltage

The capacitance reported in Table I, is the settled capacitance calculated from second current peak and beyond. However, as mentioned in Section III-A1, initial capacitance value is higher as noted from higher time period between first two peaks as compared to subsequent peak time intervals. This is due to the change in PV panel voltage from open circuit value to zero, which is defined as  $\Delta V_c$ . To see the variation in capacitance as a function of voltage, for different PV array configurations, Table IV is presented. It can be observed from Table IV that capacitance variation with voltage is in the range of 1.1 to 2.2 nF/V per panel. And the ratio  $\frac{\Delta C}{\Delta V}$  is positive, implying capacitance increases with voltage. This is in agreement with the reported literature [5].

#### F. Variation in capacitance with irradiation

Short circuit current of a solar cell is an indicative of its irradiation [11]. For same PV array configuration, capacitance is measured under different light conditions, as indicated by

the short circuit current. The difference in the short circuit current for these two different light conditions is defined as  $\Delta I_{sc}$ . The values are tabulated in Table V, where case V represents 14 PV panels connected in parallel. It can be

TABLE V: Change in array capacitance  $C_{eq}$  with irradiation  $G$  for different PV array configurations

PV array	$C_{eq_{low}G}$	$C_{eq_{high}G}$	$\Delta I_{sc}$	$\frac{\Delta C_{eq}}{\Delta I_{sc}}$
III	1.2 $\mu F$	1.6 $\mu F$	22.8 - 8.1 A	0.027 $\mu F/A$
IV	0.7 $\mu F$	1.3 $\mu F$	29.2 - 8.4 A	0.028 $\mu F/A$
V	1.9 $\mu F$	2.6 $\mu F$	61 - 40 A	0.033 $\mu F/A$

observed from Table V that change in capacitance as a function of irradiation is close to 0.03  $\mu F/A$ , however exact variation is a function of irradiation value. This sensitivity of capacitance with irradiation is considered in  $F/A$  as the short circuit current level is proportional to irradiation level [11]. The PV panel capacitance is higher at higher irradiation conditions.

#### IV. EFFECT OF CAPACITANCE ON INRUSH CURRENT

The effect of equivalent array capacitance on inrush current can be seen by evaluating the ratio of peak inrush current to short circuit current value or the normalised inrush current, for different array configurations as shown in Table VI. It

TABLE VI: Effect of array capacitance on normalised inrush current

PV configuration	$C_{eq_{initial}}$	$\frac{I_{max}}{I_{sc}}$
I	104 nF	3.4
II	67 nF	3.5
III	1200 nF	2.8
IV	700 nF	2.6

can be seen that for higher capacitance value, ratio of peak to steady current is lower. Capacitance value is higher for parallel panel case, where short circuit current is also higher. Therefore even though the ratio of peak to steady current is lower, the absolute value of peak inrush current is much higher in parallel connection of PV modules. This observation can further be extended to irradiation variation of capacitance, wherein it is seen that due to increase in irradiation, capacitance increases, reducing peak to steady current ratio. But due to increase in the short circuit current due to irradiation, absolute value of the peak current is even higher.

#### V. LIMITATIONS IN MEASUREMENTS

Practical aspects of the PV array installation causes limitations in the impedance estimation. Voltage and current waveforms are measured at roof bus bar terminal as shown in Fig. 4. Due to this, the capacitance calculated, not only reflects the PV panel capacitance but also includes the effect of cable capacitance. As cable impedance varies for different series and parallel panel connections, direct scaling in inductance and capacitance values were not observed as the cable length from the roof top bus bar to individual panels vary. These cables have lengths varying from 2 m to 6 m. Therefore these results cannot be extrapolated in general, however the presented method can be used for calculating effective R, L and C values for any system.

#### VI. CONCLUSION

Capacitance of a solar cell is important for dynamic modelling of a PV array. The capacitance is estimated based on experimental measurements. An external capacitor is connected across the terminals of a PV array. This produces a second order response, the validity of which is checked using a small signal model. From the second order response, cable resistance, inductance and PV array capacitance has been calculated. It has been observed that resistance, inductance and capacitance values scale up and down, depending upon the series and parallel combination of PV panels. However, due to the effect of connecting cable impedance, exact scaling is not observed. PV capacitance is seen to change with irradiation at the rate of 30 nF/A, where short circuit current of the PV array is used to indicate the irradiation level. Effect of voltage variation is also seen on the capacitance of PV array, which varies from 1.1 nF/V to 2.2 nF/V, depending on the voltage level and array configuration. Due to high open circuit voltage, capacitance is seen to be higher initially and it is this capacitance value that determines the peak value of the inrush current. The analysis and parameter measurements have been carried out on a variety of PV array configurations and the results are observed to be consistent.

This analysis can further be extended to derive analytical expression of inrush current and PV terminal voltage, when the PV system is connected to a power electronic inverter.

#### REFERENCES

- [1] Filippo Spertino et al., "PV Module Parameter Characterization From the Transient Charge of an External Capacitor", *IEEE J. Photovoltaics*, vol. 3, no. 4, pp. 1325-1333, Oct. 2013.
- [2] Wenjie Chen et al., "Numerical and Experimental Investigation of parasitic edge capacitance for Photovoltaic Panel", *Proc. Int. Conf. Power Electron.*, Hiroshima, Japan, May 2014, pp. 2967-2971.
- [3] R. A. Kumar et al., "Measurement of AC parameters of gallium arsenide (GaAs/Ge) solar cell by impedance spectroscopy," *IEEE Trans. Electron Devices*, vol.48, no.9, pp. 2177-2179, Sep 2001.
- [4] Katherine A. Kim et al., "A Dynamic Photovoltaic Model Incorporating Capacitive and Reverse-Bias Characteristics", *IEEE J. Photovolt.*, vol. 3, no. 4, pp. 1334-1341, Oct 2013
- [5] R. Anil Kumar et al., "Effect of Solar Array Capacitance on the Performance of Switching Shunt Voltage Regulator", *IEEE Trans. Power Electron.*, vol. 21, no. 2, pp. 543-548, Mar 2006.
- [6] P. H. Mauk et al., "Interpretation of Thin-Film Polycrystalline Solar Cell Capacitance", *IEEE Trans. Electron Devices*, vol. 37, no. 2, pp. 422-427, Feb 1990.
- [7] P. Merhej et al., "Effect of Capacitance on the Output Characteristics of Solar Cells", in *Proc. 6th Conf. Ph.D. Res. Microelectron. Electron.*, Berlin, Germany, 2010, pp. 14.
- [8] H. Mandal, "An Improved Technique of Capacitance Measurement of Solar Cells", *Proc. 3rd Conf. Computer, Communication, Control and Information Technology*, Feb. 2015, pp. 1-4.
- [9] F. Recart and A. Cuevas, "Application of Junction Capacitance Measurements to the Characterization of Solar Cells", *IEEE Trans. Electron Devices*, vol. 53, no. 3, pp. 442-448, Mar 2006.
- [10] Chatterjee, A.; Keyhani, A.; Kapoor, D., "Identification of Photovoltaic Source Models," *IEEE Trans. Energy Convers.*, vol.26, no.3, pp. 883-889, Sept. 2011.
- [11] P. Bharadwaj and V. John, "Design, Fabrication and Evaluation of Solar Irradiation Meter," *Proc. PEDES*, pp. 248-254, Dec. 2014.
- [12] P. Bharadwaj, "PV Panel Characterisation, MPPT, and Development of a Solar Irradiation Meter," ME Thesis, Dept. of EE, IISc, 2014.
- [13] *Miniature Circuit-breakers*. S 280 series 80-100 A. ABB. Sep 2015.
- [14] *Photovoltaic Module*. ES 275-295 P72. EMMVEE Photovoltaics. Sep 2012.